6. J. Homan *et al.*, *Astrophys. J. Suppl. Ser.* **132**, 377 (2001).
7. D. Hannikainen *et al.*, *Astrophys. Space Sci. Rev.* **276**, 45 (2001).
8. J. A. Orosz *et al.*, *Astrophys. J.* **568**, 845 (2002).
9. J. Swank, E. Smith, C. Markwardt, *Int. Astron. Union Circ. No. 7792* (2002).
10. S. Corbel, R. P. Fender, A. K. Tzioumis, *Int. Astron. Union Circ. No. 7795* (2002).
11. D. Hannikainen, personal communication.
12. S. Corbel *et al.*, *Astrophys. J.* **554**, 43 (2001).
13. R. P. Fender *et al.*, *Mon. Not. R. Astron. Soc.* **304**, 865 (1999).
14. T. Kotani *et al.*, *Astrophys. J.* **543**, L133 (2000).
15. M. Rupen, personal communication.
16. I. F. Mirabel, L. F. Rodríguez, B. Cordier, J. Paul, F. A. Lebrun, *Nature* **358**, 215 (1992).
17. L. F. Rodríguez, I. F. Mirabel, J. Martí, *Astrophys. J.* **401**, L15 (1992).
18. F. Seward, J. Grindlay, E. Seaquist, W. Gilmore, *Nature* **287**, 806 (1980).
19. M. G. Watson, R. Willingale, J. E. Grindlay, F. D. Seward, *Astrophys. J.* **273**, 688 (1983).
20. W. Brinkmann, B. Aschenbach, N. Kawai, *Astron. Astrophys.* **312**, 306 (1996).
21. S. Safi-Harb, H. Oegelman, *Astrophys. J.* **483**, 868 (1997).
22. S. Safi-Harb, R. Petre, *Astrophys. J.* **512**, 784 (1999).
23. G. M. Dubner, M. Holdaway, W. M. Goss, I. F. Mirabel, *Astron. J.* **116**, 1842 (1998).
24. H. L. Marshall, C. R. Canizares, N. S. Schulz, *Astrophys. J.* **564**, 941 (2002).
25. S. Migliari, R. P. Fender, M. Méndez, *Science* **297**, 1673 (2002).
26. B. J. Sams, A. Eckart, R. Sunyaev, *Nature* **382**, 47 (1996).
27. A. S. Wilson, A. J. Young, P. L. Shopbell, *Astrophys. J.* **547**, 740 (2001).
28. R. M. Sambruna *et al.*, *Astrophys. J.* **549**, L161 (2001).
29. R. M. Sambruna *et al.*, *Astrophys. J.* **571**, 206 (2002).
30. P. E. Hardee, *Astrophys. J.* **533**, 176 (2000).
31. M. J. Rees, P. Meszaros, *Astrophys. J.* **430**, L93 (1994).
32. C. R. Kaiser, R. Sunyaev, H. C. Spruit, *Astron. Astrophys.* **356**, 975 (2000).
33. R. M. Hjellming, K. J. Johnston, *Astrophys. J.* **328**, 600 (1988).
34. R. P. Fender, *Mon. Not. R. Astron. Soc.* **322**, 31 (2001).

35. S.C. and J.A.T. acknowledge useful conversations with A. Celotti, S. Heinz, and V. Dhawan. P.K. acknowledges useful discussions with H. Falcke and D. Harris. S.C. thanks C. Bailyn, S. Chaty, D. Hannikainen, and D. Hunstead for providing information before publication; F. Mirabel for a careful reading of this manuscript; and R. Ekers, D. McConnell, R. Norris, B. Sault, and the ATCA Time Allocating Committee for allowing the radio observations. We thank H. Tananbaum for granting Director's Discretionary Time for the Chandra observations and J. Nichols for rapid processing of the data. We have made use of observations performed with the European Southern Observatory (ESO) Melipal Telescope at the Paranal Observatory under Director's Discretionary Time program 268.D-5771. The Australia Telescope is funded by the Commonwealth of Australia for operation as a National Facility managed by CSIRO.

8 July 2002; accepted 26 August 2002

Condensation of Semiconductor Microcavity Exciton Polaritons

Hui Deng,[1]* Gregor Weihs,[1,2] Charles Santori,[1] Jacqueline Bloch,[3] Yoshihisa Yamamoto[1,4]

A phase transition from a classical thermal mixed state to a quantum-mechanical pure state of exciton polaritons is observed in a GaAs multiple quantum-well microcavity from the decrease of the second-order coherence function. Supporting evidence is obtained from the observation of a nonlinear threshold behavior in the pump-intensity dependence of the emission, a polariton-like dispersion relation above threshold, and a decrease of the relaxation time into the lower polariton state. The condensation of microcavity exciton polaritons is confirmed.

The search for the macroscopic quantum coherence formed in a degenerate Bose gas drives the worldwide work on atom Bose-Einstein condensation (BEC). Though the observed first order coherence of atoms is a direct manifestation of the wave nature of matter, only second-order and higher-order coherence functions can distinguish quantum-mechanical pure states from a classical thermal mixed state (*1*). In quantum optics, quantum phase transitions have been studied extensively for lasers and parametric oscillators via the second order coherence function. For atomic BECs, the second- and third-order coherence functions have been measured indirectly in the spatial domain (*2*, *3*) but not in the time domain. Semiconductor exciton polaritons constitute another promising system to explore the physics of degenerate Bose gases, but in a stronger interaction regime (*4*, *5*). However, conclusive evidence of condensation of excitons or polaritons has been elusive. We have obtained evidence for the formation of macroscopic quantum coherence by measuring the time domain of second-order coherence function $g^{(2)}(\tau)$ of the light emitted from the polaritons

$$g^2(\tau) = \frac{\langle \hat{E}^{(-)}(t)\hat{E}^{(-)}(t+\tau)\hat{E}^{(+)}(t+\tau)\hat{E}^{(+)}(t)\rangle}{\langle \hat{E}^{(-)}(t)\hat{E}^{(+)}(t)\rangle^2} \quad (1)$$

where $\hat{E}^{(-)}(t)$ and $\hat{E}^{(+)}(t)$ are the negative and positive frequency parts of the electric field operator at time t, respectively (*1*).

When the optical field of a semiconductor microcavity strongly couples to the heavy-hole excitons in embedded quantum wells (QWs) (Fig. 1A), new normal modes are formed, the lower polariton (LP) and the upper polariton (UP) (*6*). The coupling strength of the interband dipole moment to the cavity optical mode determines the splitting between the UP and LP energies. The confinement of the excitons in a QW lifts the degeneracy of the heavy-hole and light-hole excitons, so that the UP and the LP are only twofold degenerate by their spins. With integer total spin, QW excitons and cavity polaritons behave as interacting bosons in the low-density regime. The exchange interaction between the excitons' fermionic constituents, electrons and holes, introduces a repulsive interaction between excitons with identical spins (*4*, *5*, *7*, *8*). This weak repulsive interaction is indispensable for the formation of exciton or polariton BECs.

In the search for polariton condensation effects, a nonlinear emission has been observed in exciton-polariton systems (*9*–*11*), but the mechanism leading to the observed nonlinearity was not clarified. Pump-probe experiments (*12*, *13*) provided evidence of the bosonic final-state stimulation and the amplification of polaritons by polariton-polariton scattering, which is also the mechanism for creating the macroscopic polariton condensation in the work presented here. In our experiments, excitons with a large transverse momentum are initially created by optical pumping. They relax by polariton-polariton scattering (through the exciton component of the wave function) and cool subsequently by phonon emission, thereby losing the coherence inherited from the pump wave and forming a real exciton-polariton population with a quasi-thermal distribution (Fig. 1B). Due to the slow phonon emission rate and fast radiative decay rate in the region of small in-plane wavenumber $k_{\|}$ region, most of the injected excitons radiatively decay before they relax to the bottom of the LP branch (the $k_{\|} = 0$ LP state). However, it is expected that above a critical pump intensity, when the LP population per mode around $k_{\|} = 0$ approaches one, the elastic scattering of two LPs into the $k_{\|} = 0$ LP and a higher-energy LP is considerably enhanced due to bosonic final-state stimulation. This stimulated LP-LP scattering is a phase coherent process, analogous to the phase coherent stimulated emission in a laser. Consequently, a macroscopic coherent population can quickly build up in the $k_{\|} = 0$ LP state, forming a condensate.

[1]Quantum Entanglement Project, ICORP, JST, Edward L. Ginzton Laboratory, Stanford University, Stanford, CA 94305, USA. [2]Institut für Experimentalphysik, Universität Wien, Vienna, Austria. [3]LPN/CNRS, Route de Nozay, 91460, Marcoussis, France. [4]NTT Basic Research Laboratories, Astugishi, Kanagawa, Japan.

*To whom correspondence should be addressed. E-mail: dhui@stanford.edu

However, the quasi-particle picture of polaritons breaks down when the exciton density exceeds the saturation limit, where the exciton decoherence rate due to exciton-phonon scattering exceeds the UP-LP splitting. The normal modes of the system then become the cavity photon and the QW exciton. In order to increase the saturation limit, we used a system with 12 GaAs quantum wells placed at the antinode positions of a GaAs/AlGaAs microcavity (Fig. 1A). In such a system, the effective exciton density per QW is reduced to one-twelfth of the total exciton density, and hence the exciton decoherence rate for a given polariton population is suppressed. Moreover, the UP-LP splitting is increased by the square root of the number of QWs (*14*, *15*). When the polariton splitting becomes comparable to the bare exciton binding energy, the effective exciton radius in the LP is also reduced dramatically (*16*). All these effects combined make the condensation of $k_{||} = 0$ lower polaritons possible before the saturation limit is reached.

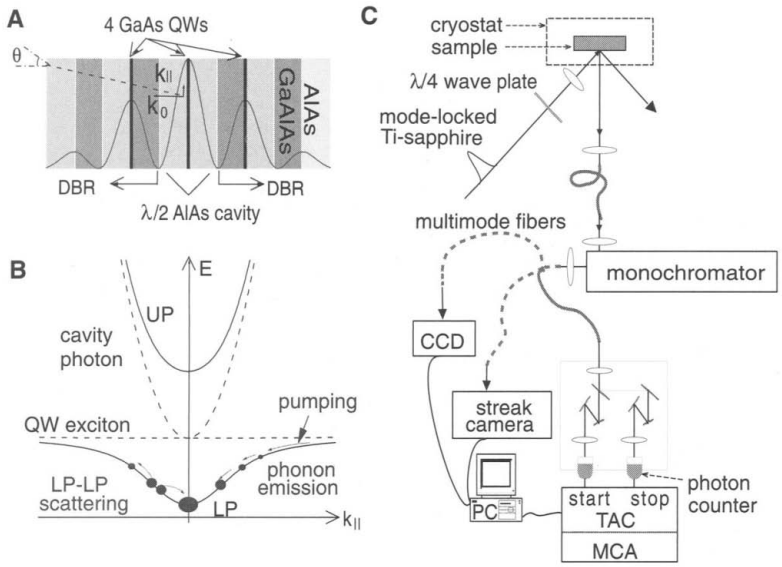

Fig. 1. Illustration of sample structure, dispersion, relaxation mechanisms, and experimental setup. (**A**) Structure of the sample consisting of a λ/2 AlAs cavity sandwiched between two distributed Bragg reflectors (DBRs), which are made of alternating $Ga_{0.8}Al_{0.2}As$/AlAs λ/4 layers. Three stacks of QWs are placed at the antinode positions of the microcavity photon field, which is depicted by the solid curve. Each stack has four 7-nm-thick GaAs QWs separated by 3-nm-thick AlAs barriers. (**B**) Dispersion curves of the QW heavy-hole exciton, cavity photon, UP, and LP. The cavity photon and QW exciton are on resonance at $k_{||} = 0$. The two relaxation mechanisms, multiple phonon emission and LP-LP scattering, are also depicted. (**C**) The experimental setup, showing the laser-excited sample (top), collecting and spectral filtering optics (middle), and HB-T type configuration (bottom).

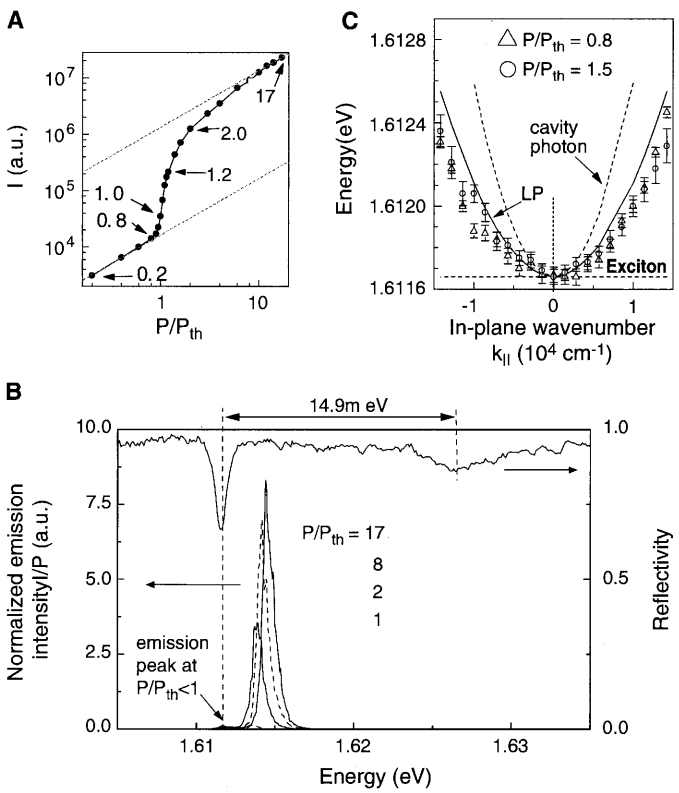

Fig. 2. Static property measurements of the emission. (**A**) Lower polariton emission intensity versus normalized pump intensity P/P_{th}. $P_{th} \approx 300$ W/cm^2. (**B**) Reflection spectrum (upper curve), and emission spectra of the LP at various pump intensities (lower curves). The relatively broad emission bandwidth is due to polariton-polariton interaction (*27*). The broad linewidth of the UP reflection spectrum, compared with the LP linewidth, is due to the background band-to-band absorption, and the increased exciton size in the UP, caused by the very strong coupling between the cavity optical mode and interband dipole moment (*16*). (**C**) Observed dispersion of the LP below and above threshold. Both curves agree with the calculated LP dispersion (solid line) and are well discriminated from the calculated QW exciton and cavity photon dispersions (dashed lines). Energy origins of the curves are shifted for easy comparison.

In all of our measurements, the sample temperature was 4 K. Reflectivity measurements gave 1.6116 eV and 14.9 meV for the bare exciton energy and the UP-LP splitting, respectively. The experimental setup is depicted in Fig. 1C. We excited the initial polariton population using a mode-locked Ti-Sapphire laser with a pulse duration of 3 ps and a repetition rate of 76 MHz. The pump was circularly polarized and focused to a spot 20 μm in diameter on the sample where the QW exciton is on resonance with the cavity photon under weak excitation. At 40° from normal incidence in air, the pump was resonant with polaritons having an in-plane wavenumber $k_{||} = 5.33 \times 10^4$ cm^{-1}. At this incidence angle, direct coherent four-wave mixing is forbidden (*17*, *18*). We collected the emitted light with an angular resolution of 1° in air using an optical fiber that was connected to an imaging spectrometer, a streak camera for time domain analysis, or a Hanbury Brown–Twiss-type (HB-T) setup for the measurement of the second order coherence function.

The emission intensity I into the normal direction is proportional to the population of the polaritons in the $k_{||} = 0$ LP state. Its dependence on the pump intensity reveals a sharp super-linear increase near the threshold (Fig. 2A), which indicates the onset of stimulated polariton-polariton scattering into the $k_{||} = 0$ LP state. The pump power density at threshold is $P_{th} \sim 300$ W/cm^2, corresponding to an excitation density of $n_{QW} = 8 \times 10^9$ cm^{-2} polaritons per pulse per QW (*19*). It is 30 times smaller than the saturation limit and more than two orders of magnitude smaller than the Mott density of 3×10^{12} cm^{-2} per QW. The total exciton population is $n_{LP} = 12 n_{QW} \sim 10^{11}$ cm^{-2} per pulse. The LP population per mode around $k_{||} = 0$, n_{LP}, at threshold is estimated to be of the order of unity (*19*). Emission spectra (Fig. 2B) feature a blue shift of the emission energy due to the phase space filling of the excitons (*20*). The maximum blue shift of 3 meV is still much less than half of the UP-LP splitting of 7.45 meV; i.e., the energy of the emission always

remains distinctly below the QW exciton and cavity photon energy. This ensures that the polariton is still the normal mode of the system.

To measure energy versus transverse wavenumber, we collected the far-field emission spectra at various external emission angles. The results are compared with the theoretical dispersion curves for the LP, cavity photon, and QW exciton (Fig. 2C). The effective mass of the quasi-particle responsible for the nonlinear emission is defined by $m_{eff} = \hbar^2(d^2E/dk_{\|}^2)$ and can be deduced from the measured dispersion curves. It is about the same below threshold and just above threshold, both in close agreement with the theoretical value. At $P/P_{th} = 17$, which is the highest pump intensity we used, m_{eff} decreased by 30% due to the blue detuning of the exciton energy with respect to the cavity photon energy as a result of the phase space filling effect described above (*20*). This is in sharp contrast to a saturated GaAs single QW microcavity system for which a transition of the effective mass from twice the photon mass to the photon mass was observed at threshold (*21*, *22*). That the measured LP mass is significantly larger than the bare photon mass is strong evidence that we have observed a polariton condensate rather than a normal photon laser.

We present the result of a time-domain measurement of the $k_{\|} = 0$ LP emission intensity detected at normal direction by a streak camera with an overall resolution of 5 ps (Fig. 3). The full width at half maximum (FWHM) and turn-on delay of the emission pulse are obtained by deconvolving the detected pump pulse from the detected emission pulse. Distinctly different from the coherent polariton four-wave mixing process (*15*, *17*, *23*), there is a finite turn-on delay and turn-off decay of the $k_{\|} \approx 0$ LP emission relative to the pump pulse. This is a signature that the optically injected polaritons relaxed into the $k_{\|} = 0$ LP state. Below threshold, the relaxation of the LPs is mainly due to slow multiple-phonon emissions, resulting in a large delay time of about 100 ps and a very long decay tail of about 350 ps. Above threshold, the stimulated LP-LP scattering accelerates the relaxation, leading to a much shorter turn-on delay and turn-off decay.

To measure the second-order coherence function, the pulsed LP emission centered at 770.8 nm was collected in the direction normal to the sample surface and was filtered by a monochromator with a resolution of $\Delta\lambda = 0.1$ nm, resulting in a pulse with a coherence time of $\Delta\tau_c = \sqrt{8 \ln 2}\, \lambda^2/(c\Delta\lambda) \sim 4$ ps. The filtered pulse was then sent to an HB-T setup (Fig. 1C). Two single photon counting modules were used for detection. The electronic pulses from the photon counters were used as start (t_1) and stop (t_2) signals for a time-to-amplitude converter (TAC), which is in turn connected to a multi-channel analyzer (MCA). The MCA records a histogram of the time intervals $t_2 - t_1$. The time resolution $T_r = 500$ ps of the photo counters is much longer than the emission pulse width in our experiment, but still much shorter than the pulse repetition period $T_{rep} = 13$ ns. Hence, the recorded histograms consist of equally spaced peaks with a width determined by T_r. The normalized peak areas are given by

$$\overline{g^{(2)}}(j) = \frac{\langle n_1(i)\, n_2(i+j)\rangle_i}{\langle n_1\rangle\, \langle n_2\rangle} \qquad (2)$$

where $n_1(i)$ and $n_2(i + j)$ are the photon numbers detected by the two photon counters in pulses i and $i + j$, respectively. In the limit of low average count rates (<0.01 per pulse in our experiment), $\overline{g^{(2)}}(j)$ approximates $g^{(2)}(\tau)$ (defined in Eq. 1) time averaged over each pulse.

Below threshold, the emission is expected to be in a multimode thermal state, for which $g^{(2)}(0) = 2$ and $g^{(2)}(\tau \gg \Delta\tau_c) = 1$ (*24*). The FWHM temporal width of the pulse is about 350 ps below threshold (Fig. 3), much longer than $\Delta\tau_c$. The measured $\overline{g^{(2)}}(0)$ (Fig. 4) is an integration of $g^{(2)}(0)$ over the whole pulse (Eq. 2) and therefore is close to 1. At threshold, the pulse width shortens to ~8 ps and is now comparable to $\Delta\tau_c$. Hence, $\overline{g^{(2)}}(0)$ is close to $g^{(2)}(0)$. Here, we observed bunching of the emitted photons, with a maximum $\overline{g^{(2)}}(0)$ of 1.77 at $P/P_{th} \sim 1.1$. This bunching effect, which is obscured by the time integration effect below threshold, is expected

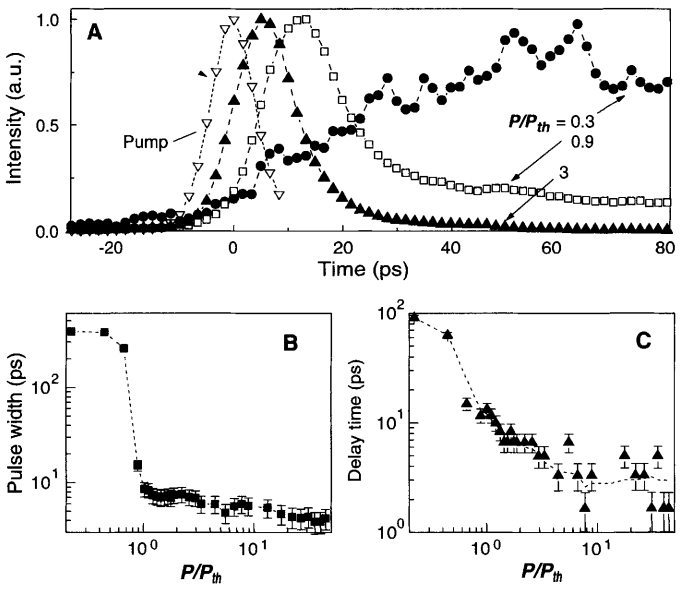

Fig. 3. Dynamic property measurement of the emission. **(A)** The time evolution of the $k_{\|} = 0$ LP emission intensity. **(B)** Pulse FWHM ΔT_p versus pump intensity P/P_{th}. **(C)** Turn-on delay time of the emission pulse versus pump intensity P/P_{th}.

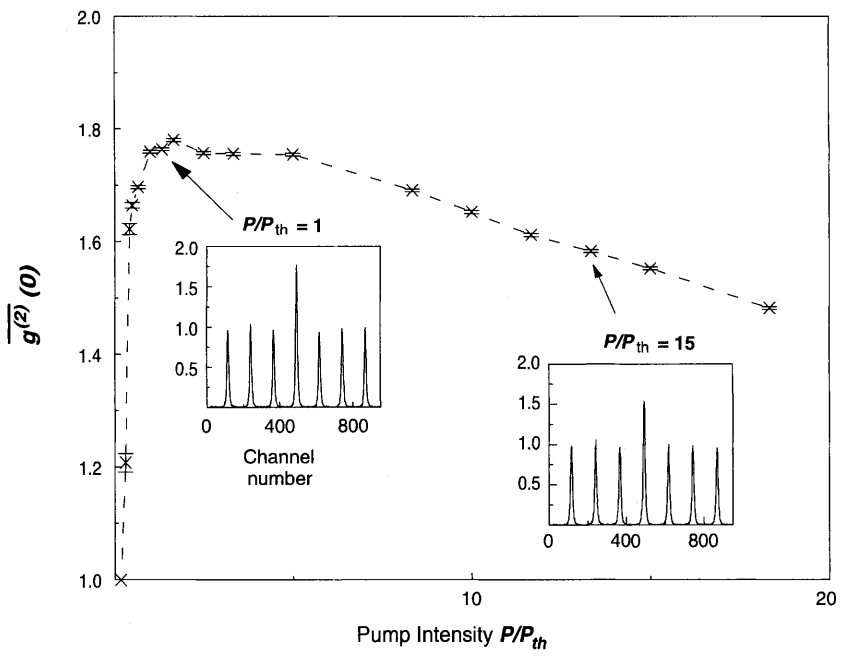

Fig. 4. The second order coherence function $\overline{g^{(2)}}(0)$ versus pump intensity P/P_{th}.

for a thermal state. Far above threshold, the pulse width only decreases further and therefore $g^{(2)}(0)$ remains a good estimate for $g^{(2)}(0)$. However the $g^{(2)}(0)$ measured in this region decreases, demonstrating that second-order coherence, or in other words, a quantum-mechanical pure state, is forming in the polariton condensate.

In conclusion, the quantum phase transition from a classical thermal mixed state to a quantum-mechanical pure state in an exciton polariton system is confirmed by observing the decrease of $g^{(2)}(0)$ above threshold. It is still an open question what specific quantum state the condensate falls into. A standard BEC theory suggests a particle number eigenstate at absolute zero temperature. The quantum Monte-Carlo wavefunction analysis based on the exciton-phonon coupling in an open system suggests a coherent state (*25*). However, the interactions among polaritons leads to virtual excitations of quantum correlated pair excited states (*26*, *27*), which resembles a squeezed state in quantum optics. For all of these cases, $g^{(2)}(0)$ is expected to approach one, so the present experiment does not distinguish among these possible quantum states. Fortunately, due to the half matter–half light nature of the polaritons (*28*), their coherence properties are transferred to the emitted light field. They then can be measured with methods well developed in quantum optics such as higher-order coherence functions and optical homodyne tomography (*29*). Future research along this line should clarify the exact nature of the quantum state that the polariton condensate approaches above threshold.

References and Notes

1. R. J. Glauber, *Phys. Rev.* **130**, 2529 (1963).
2. W. Ketterle, H. J. Miesner, *Phys. Rev. A* **56**, 3291 (1997).
3. E. A. Burt *et al.*, *Phys. Rev. Lett.* **79**, 337 (1997).
4. A. Griffin, D. W. Snoke, S. Stringari, *Bose-Einstein Condensation* (Cambridge Univ. Press, Cambridge, 1995).
5. S. A. Moskalenko, D. W. Snoke, *Bose-Einstein Condensation of Excitons and Biexcitons and Coherent Nonlinear Optics with Excitons* (Cambridge Univ. Press, New York, 2000).
6. C. Weisbuch, M. Nishioka, A. Ishikawa, Y. Arakawa, *Phys. Rev. Lett.* **69**, 3314 (1992).
7. M. Kuwata-Gonokami *et al.*, *Phys. Rev. Lett.* **79**, 1341 (1997).
8. F. Tassone, Y. Yamamoto, *Phys. Rev. B* **59**, 10830 (1999).
9. L. S. Dang, D. Heger, R. André, F. Boeuf, R. Romestain, *Phys. Rev. Lett.* **81**, 3920 (1998).
10. P. Senellart, J. Bloch, *Phys. Rev. Lett.* **82**, 1233 (1998).
11. G. Dasbach, T. Baars, M. Bayer, A. Larionov, A. Forchel, *Phys. Rev. B* **62**, 13076 (2000).
12. R. Huang, F. Tassone, Y. Yamamoto, *Phys. Rev. B* **61**, R7854 (2000).
13. R. Huang *et al.*, *Phys. Rev. B* **65**, 165314 (2002).
14. J. Bloch, T. Freixanet, J. Marzin, V. Thierry-Mieg, R. Planel, *Appl. Phys. Lett.* **73**, 1694 (1998).
15. M. Saba *et al.*, *Nature* **414**, 731 (2001).
16. J. B. Khurgin, *Solid State Commun.* **117**, 307 (2000).
17. J. J. Baumberg *et al.*, *Phys. Rev. B* **62**, R16247 (2000).
18. C. Ciuti, P. Schwendimann, A. Quattropani, *Phys. Rev. B* **63**, R041303 (2001).
19. n_{QW} is estimated from the number of pump photons per pulse ($\sim 5 \times 10^7$) multiplied by the absorption per quantum well ($\sim$1%) and the percentage of the pump light coupled into the microcavity ($\sim$5%). For a spot of $D \approx 20$ μm in diameter, $n_{QW} \approx 8 \times 10^9$ cm^{-2} per pulse. n_{LP} at threshold is estimated to be $\sim$1 by $N_{LP} = n_{LP} M \eta f_P \Delta T_P / \tau_{LP}$ with the following parameters: the detected photon flux $N_{LP} = 2500$ s^{-1}, the repetition rate of the mode-locked pump laser $f_P = 76$ MHz , the overall detection efficiency $\eta \sim 10^{-4}$, the emitted pulse duration $\Delta T_P \sim 10$ ps, LP lifetime $\tau_{LP} \sim 3$ ps, and $M = \frac{1}{2} \frac{\pi D^2/4}{4\pi^2} \frac{\pi(k_0 \Delta\theta)^2}{4}$ is the number of transverse states subtended by the acceptance angle of the detector $\Delta\theta \sim 0.01$. $k_0 = 8.15 \times 10^4$ cm^{-1} is the freespace logitudinal wavenumber of the cavity photon.
20. C. Ciuti, P. Schwendimann, B. Deveaud, A. Quattropani, *Phys. Rev. B* **62**, R4825 (2000).
21. H. Cao *et al.*, *Phys. Rev. A* **55**, 4632 (1997).
22. M. Kira *et al.*, *Phys. Rev. Lett.* **79**, 5170 (1997).
23. P. G. Savvidis *et al.*, *Phys. Rev. Lett.* **84**, 1547 (2000).
24. C. W. Gardiner, P. Zoller, *Quantum Noise* (Springer-Verlag, New York, 2000).
25. A. Imamoglu, R. Ram, *Phys. Lett. A* **214**, 193 (1996).
26. M. Naraschewski, R. J. Glauber, *Phys. Rev. A* **59**, 4595 (1999).
27. F. Tassone, Y. Yamamoto, *Phys. Rev. A* **62**, 063809 (2000).
28. Y. Yamamoto, *Nature* **405**, 629 (2000).
29. D. Smithey, M. Beck, M. Raymer, A. Faridani, *Phys. Rev. Lett.* **70**, 1244 (1993).

29 May 2002; accepted 29 August 2002

Dynamics of Hydrogen Bromide Dissolution in the Ground and Excited States

S. M. Hurley, T. E. Dermota, D. P. Hydutsky, A. W. Castleman Jr.*

The dissolution of acids is one of the most fundamental solvation processes, and an important issue is the nature of the hydration complex resulting in ion pair formation. We used femtosecond pump-probe spectroscopy to show that five water molecules are necessary for complete dissolution of a hydrogen bromide molecule to form the contact ion pair $H^+ \cdot Br^-(H_2O)_n$ in the electronic ground state. In smaller mixed clusters ($n < 5$), the ion pair formation can be photoinduced by electronic excitation.

In many areas of atmospheric and biological chemistry, the dissolution of acids in aqueous media is of fundamental importance. One of the basic processes of interest is the acid ionization of hydrogen bromide (HBr) molecules in aqueous media to form the contact ion pair $H^+ \cdot Br^-$, which has been the subject of many theoretical studies (*1–5*) but relatively few experimental studies (*6*). One extensively discussed issue is the minimum number of water molecules that is necessary to solvate the molecule and form the contact ion pair in isolated complexes. Theoretical calculations (*1–3*) predict that contact ion pair formation starts to occur in the mixed cluster containing three water molecules, and by the $n = 4$ mixed cluster, complete dissolution has occurred. Here, we report an investigation into the ultrafast dynamics of mixed clusters of HBr-water, using the pump-probe technique (*7*) coupled with reflectron time-of-flight mass spectrometry (*8*, *9*) to determine the mechanism of ion pair formation in the ground and excited electronic states of HBr.

A molecular beam composed of HBr clusters was formed by the supersonic expansion through a pulsed nozzle (150 μm in diameter) of a 10% HBr (Matheson gas) mixture seeded in argon maintained at a total backing pressure of ~3 bar. Mixed HBr-water clusters were formed by crossing the neutral cluster beam with an effusive water vapor beam from a pickup source (*10*). A (2 + 1) pump-probe ionization scheme (pump, 271 nm; probe, 407 nm; pulse duration, 80 fs) was used to study the dynamics of HBr-water clusters excited to the $v = 1$ level of the Rydberg $C^1\Pi$ state of the HBr chromophore (*11*). Mass spectra revealed a typical cluster distribution, including HBr clusters up to size 10, $H^+(H_2O)_n$ (n = 1 to 4) and mixed clusters of $H^+(HBr)(H_2O)_n$ (n = 1 to 3). In Fig. 1A, the pump-probe temporal responses of HBr^+ and H_2O^+ are shown. The transient pump-probe dynamics of the protonated water clusters (Fig. 1B) are substantially different from those of the HBr^+ and H_2O^+ monomers (Fig. 1A). The $H^+(H_2O)_n$ originate from a mixed cluster of HBr and water. The excess proton in the product originates from the HBr, as established through extensive studies of the isotopically substituted acids. After ionization of the mixed cluster, a neutral bromine is lost, and only protonated water clusters are detected, as depicted in Eq. 1.

$$HBr(H_2O)_n + (2+1)h\nu \rightarrow H(H_2O)_n^+ + Br + e^- \quad (1)$$

where h is Planck's constant and ν is frequency. Under the conditions of the present experiments, water is added effusively, and neutral water clusters are not formed; hence,

Departments of Chemistry and Physics, Pennsylvania State University, University Park, PA 16802, USA.

*To whom correspondence should be addressed. E-mail: awc@psu.edu